Article

pubs.acs.org/Biomac

Swelling and Free-Volume Characteristics of TEMPO-Oxidized Cellulose Nanofibril Films

Jonathan Ø. Torstensen,[†] Ming Liu,[‡] Soo-Ah Jin,[§] Liyuan Deng,[†] Ayman I. Hawari,[‡] Kristin Syverud,[†,∥] Richard J. Spontak,*[,§,⊥] and Øyvind W. Gregersen*[,†,∥]

[†]Department of Chemical Engineering, Norwegian University of Science and Technology, 7491 Trondheim, Norway

[‡]Department of Nuclear Engineering, North Carolina State University, Raleigh, North Carolina 27695, United States

[§]Department of Chemical & Biomolecular Engineering, North Carolina State University, Raleigh, North Carolina 27695, United States

[∥]RISE PFI AS, 7491 Trondheim, Norway

[⊥]Department of Materials Science & Engineering, North Carolina State University, Raleigh, North Carolina 27695, United States

ABSTRACT: Cellulose nanofibrils (CNFs) are becoming increasingly ubiquitous in diverse technologies requiring sustainable nanoscale species to form or modify films. The objective of the present study is to investigate the swelling behavior and accompanying free volume of self-standing TEMPO-oxidized (TO) CNF films in the presence of water vapor. For this purpose, we have performed time-resolved swelling experiments on films, prepared according to different experimental protocols, at 90% relative humidity (RH) and ambient temperature. Corresponding free-volume characteristics are elucidated by positron annihilation lifetime spectroscopy (PALS) conducted at ambient temperature and several RH levels. Increasing the drying temperature of the films (from ambient to 50 °C) is observed to promote an increase in film density, which serves to reduce bulk swelling. These elevated drying temperatures likewise cause the free-volume pore size measured by PALS to decrease, while the corresponding total free-volume fraction remains nearly constant. Similarly, dispersion of TO-CNF into aqueous suspensions by ultrasonication prior to film formation increases both the total free-volume fraction and pore size but reduces the size of individual nanofibrils with little net change in bulk swelling. The swelling and concurrent free-volume measurements reported here generally reveal an increase in the free volume of TO-CNF films with increasing RH.

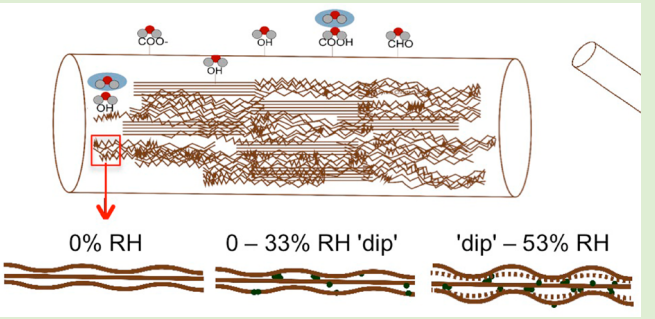

INTRODUCTION

Cellulose nanofibrils (CNFs) surface-modified in the presence of 2,2,6,6-tetramethyl-piperidin-1-yl)oxyl, referred to as TEMPO (TO), have become increasingly popular since their inception in 2006.[1] Since that time, TO-CNF has been considered for use in a wide variety of technologies as, for instance, a functional paper additive,[2] an air-filter precursor,[3] a biomedical device component,[4] and a polymer composite additive to improve mechanical properties.[5] Production of TO-CNF from sustainable wood resources is commonly achieved in a two-step process: TEMPO-mediated oxidation, followed by mechanical agitation to isolate the CNFs.[6] While the starting material is routinely cellulose pulp originating from a broad range of sources, the final material consists of nano/microfibrils possessing a net negative surface charge due to the presence of carboxyl groups, which promote hydrophilicity. TEMPO treatment selectively oxidizes these hydroxyl groups to carboxylic moieties, resulting in a stronger negative surface charge and enhanced hydrophilicity. Depending on the oxidation conditions, the carboxylic acid content can be as high as ∼1.6 mmol/g.[7] Mechanical agitation introduces disruptive shear forces through the use of homogenization, sonication, or microfluidization and generates CNFs typically possessing the same crystallinity as the starting pulp[7] and measuring 1.6−3.8 nm in width[8,9] and ranging from several hundred nanometers[10] up to several micrometers in length.[11] Due to their high aspect ratio and to facilitate analysis, TO-CNFs are often schematically portrayed as rods (cf. Figure 1). A molecular-level study[12,13] of CNF dissolution reveals that nanofibrils possessing a square cross section measuring 5.2 nm across contain 36 chains, thereby yielding ∼1.3 chains/nm^2. Atomic force microscopy (AFM) images of the present TO-CNF (an example of which is included in Figure 1) indicate that the nanofibrils measure 2.37 ± 0.65 nm in diameter (measured in triplicate on 15 TO-CNFs) or, alternatively, 4.4 nm^2 on average in cross-sectional area. The corresponding number of chains/nanofibrils is therefore estimated to be ∼6.

Received: December 22, 2017
Revised: January 19, 2018

DOI: 10.1021/acs.biomac.7b01814
Biomacromolecules XXXX, XXX, XXX−XXX

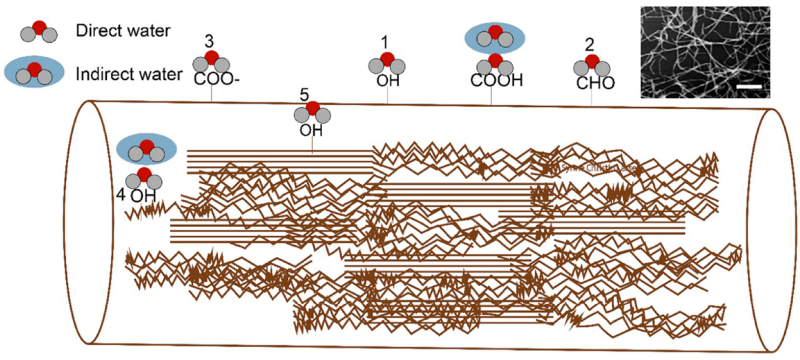

Figure 1. Schematic illustration of water sorption in a TEMPO-oxidized cellulose nanofibril (TO-CNF) film. Sorption occurs as water binds primarily to external hydroxyl, aldehyde, and carboxylic groups (1−3) in internal amorphous regions (4) and along crystalline facets (5). A representative AFM image of the TO-CNF is provided in the inset (scale bar = 200 nm).

We recognize that hierarchical structures, including (partial) plant cells, might also be present.[14,15]

Films composed of TO-CNF are relatively straightforward to prepare but nontrivial to analyze. Of particular interest in the present work is the swelling behavior of such hygroscopic films in the presence of water vapor, since they are likely to be used in environments varying in relative humidity (RH). As described in more detail below, bulk swelling under these conditions has been extensively studied. In this work, however, we focus on the accompanying changes in TO-CNF free volume. Free volume generally refers to the unoccupied space between polymer chains[16] and, when modeled as spherical pores, is expected to measure on the order of a few angstroms from equation-of-state considerations of small molecules.[17] This concept, introduced to explain the glassy behavior of amorphous polymers, is rooted in the entropic contribution[18] to statistical thermodynamics.[19] Free volume is associated with the amorphous regions of a polymer,[20] in which case an increase in polymer crystallinity proportionately decreases the available free volume, which governs bulk properties such as the glass transition temperature (T_g) and melt viscosity, as well as the diffusive transport of molecular penetrants.[17] While free volume can be indirectly measured from PVT (pressure−volume−temperature) or viscosity data, it can also be accurately estimated from various group contribution methods. Since the 1990s, however, positron annihilation lifetime spectroscopy (PALS) has gained increasing popularity as an analytical tool that is capable of directly measuring free volume in polymer films and composites.[17,21] General observations to date indicate that the free-volume pores (possessing a presumed spherical shape) present in many polymers measure 0.4−1.0 nm in diameter.[22−25]

Of particular interest in the present study is the use of PALS to explore the free volume of TO-CNF films.[24] In this case, the diameter of spherical free-volume pores has been reported to be 0.47 nm, irrespective of position across film thickness under vacuum. The use of evacuated conditions, however, altogether precludes exposure to water vapor, which has been investigated by PALS in conjunction with a variety of hydro/amphiphilic polymeric materials, including poly(vinyl alcohol),[26] epoxies,[27,28] cellulose acetate,[25] and copolymers.[25] At low RH levels, some of these systems are observed to experience a decrease in average free-volume size that is lower than that measured at 0% RH. This initial reduction has been attributed to a molecular-level mechanism wherein water molecules fill existing free-volume pores before the pores are forced to expand at higher RH levels. In this study, TO-CNF films produced by different fabrication methods are characterized to reveal differences in film structure, macroscopic swelling, and free volume due to the presence of water vapor. Here, we have developed an experimental protocol that permitted direct measurement of free volume at systematically varied RH levels, which has not been previously reported to the best of our knowledge with regard to TO-CNF films. The molecular-level role of water discerned from resultant PALS data under these conditions is interpreted to explain the mechanism of TO-CNF film swelling.

Water Sorption Kinetics. Cellulose, as well as TO-CNF, is a hygroscopic material, indicating that it naturally remains in thermodynamic equilibrium with surrounding water vapor or liquid.[29] This equilibrium is complex and thoroughly investigated for different types of cellulose,[30] as well as for cellulose in composites.[31] Moreover, cellulosic materials are prone to water-sorption hysteresis,[32] which relates the measured moisture content to the method by which the material is conditioned in a moist or liquid environment prior to measurement. When water uptake of hygroscopic cellulosic materials is under consideration, it necessarily includes both absorption and adsorption. Nanocellulose, of which TO-CNF constitutes an example, does not possess a clearly defined exterior surface, implying that both sorption mechanisms occur simultaneously. In addition, sorption can be classified as either slow or fast,[33] depending on the chemical makeup and spatial location of the binding species. For instance, sorption occurs quickly in TO-CNF films as water binds to surface hydroxyl and carboxylic groups. Conversely, water molecules bind more slowly to internal amorphous moieties and crystalline facets (water cannot penetrate the crystallites[34]). A distinction is also made between direct sorption, which corresponds to water molecules that hydrogen-bond directly to CNFs, and indirect sorption, wherein water molecules bind to other, already bound water molecules.

Other considerations that must be considered in water sorption and TO-CNF film swelling[6] are interfibril interactions, which can inhibit swelling under the following conditions: (i) the volume increase of a hydrated nanofibril is physically hindered by other nanofibrils in the network, and (ii) water binding competes with interfibril binding for available hydrogen bonds. Since water sorption in TO-CNF films follows a bimechanistic process (e.g., fast vs slow, direct vs indirect, and water binding vs interfibril binding), a model that is commonly used to describe the water sorption kinetics for cellulosic films

DOI: 10.1021/acs.biomac.7b01814
Biomacromolecules XXXX, XXX, XXX−XXX

is the parallel exponential kinetics (PEK) model.[35] This model derives from the presumption that the mass gain at a given time (t) during swelling at a specific RH (M_t) is the sum of two parallel swelling processes, each with its own time constant (α_1 or α_2), as indicated by

$$M_t = M_{\infty 1}(1 - e^{-t/\alpha_1}) + M_{\infty 2}(1 - e^{-t/\alpha_2}) \quad (1)$$

Equation 1 can be interpreted as the occurrence of two concurrent sorption processes with each capable of reaching its equilibrium water solubility ($M_{\infty 1}$ and $M_{\infty 2}$). The processes in the PEK model possess nominally fast (α_1) and slow (α_2) characteristic times, and the corresponding sorption sites are schematically depicted in Figure 1. While precise categorization of different sorption sites as fast or slow has yet to be conclusively established[36] in terms of their relation to specific terms in eq 1,[30,33,35] the time constants are material-specific and can be extracted from sorption experiments performed at different RH levels.[30]

Positron Annihilation Lifetime Spectroscopy. Since PALS remains a largely specialized characterization technique, we briefly describe its underlying principle and analysis methodology in this section. The technique uses positrons (electron antiparticles) as a probe by which to characterize vacancy defects and free-volume voids in a wide range of inorganic and organic materials. Detailed reviews of PALS are available elsewhere.[12,32] When positrons are implanted into a subject material, they tend to diffuse and become trapped in such vacancies and voids, and eventually annihilate with surrounding electrons. In a typical bulk system subjected to PALS analysis that employs ^{22}Na as the positron source, the birth of a positron is marked as the start signal by detection of coincident γ radiation of 1274 keV, whereas the decay of the positron is signaled by detection of annihilation γ rays of 511 keV, which effectively serves as the stop signal. By recording the temporal intensity (I) histogram between the start and stop signals, a PALS spectrum is obtained. Such spectra frequently consist of several exponential decay components of the form

$$I(t) = \sum_{j=1}^{n} I_j \exp\left(-\frac{t}{\tau_j}\right) \quad (2)$$

where I_j and τ_j denote the intensity (or number-density population) and lifetime of the jth annihilation lifetime component, respectively.

In polymers and semiconductors, positrons might also form positronium (Ps) species (a metastable bound state of a positron and an electron) that also undergo annihilation. The alignment of the electron and positron spins dictates whether Ps is in a singlet state (*para*-positronium or p-Ps) or a triplet state (*ortho*-positronium or o-Ps). Since the first two lifetimes (τ_1 and τ_2) in eq 2 correspond to positron and/or p-Ps annihilation and are only related to fast processes that are relatively short, their analysis is not relevant in the present study. Of particular importance in this study is the o-Ps lifetime, which can be correlated with the free-volume pore size of polymers, thereby revealing the morphological features of polymeric media at atomic length scales. Although o-Ps ions possess a lifetime of 142 ns in vacuum, this lifetime can be significantly shortened within materials through a pick-off process wherein the positron annihilates an environmental electron (from the polymer) instead of its original pair. This shortened o-Ps lifetime (τ_3) can be directly related to the free-volume pore size through such correlations as the Tao–Eldrup model,[37,38] expressed as

$$\tau_3 = 0.5\left(1 - \frac{r}{r + \Delta r} + \frac{1}{2\pi}\sin\left(\frac{2\pi r}{r + \Delta r}\right)\right)^{-1} \quad (3)$$

where r represents the radius of a spherical free-volume pore and Δr (=0.166 nm) accounts for the electron shell extending into the free-volume pore.[39] While this model is commonly used to extract free-volume characteristics from polymers, other models, including those not restricted to specific shapes, have been proposed. In the present work, a shape-free model[40] that cannot be expressed in closed form due to its quantum-mechanical derivation has been utilized for analysis purposes. Moreover, the associated intensity of the o-Ps component (I_3) in eq 2 provides the relative number density of free-volume elements[41] among only similar material systems, since this quantity is sensitive to material chemistry. When comparing PALS results acquired from the same material series, however, the total volume (L) of the free-volume elements, approximated as spherical in shape, can be obtained from

$$L = I_3 \times \frac{4}{3}\pi r^3 \quad (4)$$

EXPERIMENTAL SECTION

Materials. Softwood (fully bleached) pulp was supplied by Södra (Växjö, Sweden) and was oxidized at ambient temperature with 98% TEMPO (Sigma-Aldrich, St. Louis, MO, USA), sodium bromide (NaBr; > 99%, Sigma-Aldrich), and sodium hypochlorite (NaClO; Roth Chemicals, Karlsruhe, Germany). Sodium hydroxide (NaOH) and hydrochloric acid (HCl) were purchased from Fisher Scientific (Hampton, NH, USA).

Methods. *1. Pulp Oxidation.* A fresh solution consisting of 1.25% w/w TEMPO/pulp and 12.5% w/w NaBr/pulp was prepared in deionized (DI) water on the day of use. The solution was added to 220 g of pulp stirred in DI water for 10 min, and the resulting suspension was diluted to 1.33 wt % prior to oxidation with 1.1 mol of NaClO gradually added in eight allotments over the course of 50 min. This corresponds to 5 mmol of NaClO/g of pulp. During this oxidation process, the pH was maintained at 10.5 by gradually adding 0.5 M NaOH. When the pH remained constant over a period of 10 min, the reaction was presumed to be completed, and the suspension was neutralized (pH 7.0) with 0.5 M HCl. The oxidized pulp was vacuum-filtered using filter paper with DI water until a conductivity of <5 μS/cm was measured and subsequently stored at 4 °C. Suspensions at 0.8 wt % concentration were homogenized with a Rannie 15 type 12.56X instrument (APV, SPX Flow Technology, Silkeborg, Denmark) operated at 600 bar for one pass, followed by a second pass at 1000 bar. The final carboxylic acid content was measured by conductiometric titration[42] as the average of three parallel trials. The acid-soluble lignin fraction was determined according to the TAPPI Useful Method 250 standard with an absorption of 205 nm and lignin extinction coefficient of 110 g/L cm. The remaining cellulose and hemicellulose contents were discerned by subjecting the suspension to acid hydrolysis, followed by high-pressure liquid chromatography (HPLC).

2. Film Preparation. A suspension composed of 400 g of 0.3 wt % TO-CNF in DI water was prepared by stirring at 1100 rpm for 60 min, followed by either direct casting or probe sonication prior to casting. Probe sonication, conducted with a 3.2 mm Qsonica probe for 10 min at 80% intensity, was performed while concurrently stirring at 1100 rpm. Specimens are hereafter designated as S (for sonicated suspension) or NS (for not sonicated suspension). Films were produced by casting 60 mL suspensions into polyethylene Petri dishes (measuring 15 mm in depth and 95 mm in diameter) and then drying at ambient temperature (20–22 °C), 35, or 50 °C in a gravity

DOI: 10.1021/acs.biomac.7b01814
Biomacromolecules XXXX, XXX, XXX–XXX

convection oven. Specimens are further denoted as Amb (dried at 20–22 °C), 35 (dried at 35 °C), or 50 (dried at 50 °C), as listed in Table 1. All films were finally dried at 80 °C for 3 h at 0.33 bar.

Table 1. Specimen Designations Employed in This Study

specimen designation	drying temperature (°C)	sonication status
Amb-NS	ambient	NS
Amb-S	ambient	S
35-NS	35	NS
35-S	35	S
50-S	50	S

3. Sample Characterization. Dynamic light scattering (DLS) was performed on TO-CNF suspensions diluted to 0.01 wt % and gently stirred for 5 min with a Malvern Nano Zetasizer. The viscosity was taken as that of water (0.89 cP), and CNF suspensions were measured for 30 runs of 30 s each for a total of 30 such measurements. These measurements were averaged to yield the reported particle size distribution. Scanning electron microscopy (SEM) of specimens cryofractured in liquid nitrogen to yield cross sections that were subsequently sputter-coated with 5 nm Au/Pd was conducted on an ultrahigh-resolution FEI Verios 460L instrument at 1.0–1.5 kV without stage bias. Samples were prepared and investigated the same day. Films intended to investigate swelling kinetics were stored in a desiccator at 0% RH for at least 16 h until the swelling tests were performed. These tests were conducted gravimetrically by exposing films to water vapor at 90 ± 2% RH and 23.9 ± 0.1 °C in a Percival climate chamber. Specimens were weighed every hour for the first 12 h and then at preselected times thereafter. All swelling experiment results reflect four replicates, and equilibrium values correspond to 96 h. Film swelling (S) was characterized by the film weights prior to swelling (W_0) and after a given time in the humidity chamber (W_t) according to

$$S = \left(\left(\frac{W_t}{W_0}\right) - 1\right) \times 100\% \quad (5)$$

The PALS measurements were performed in the presence of an ~10 μCi ^{22}Na source sealed between Kapton films measuring 7.6 μm thick. Two Hamamatsu 3378-50 photomultiplier tubes with plastic scintillators (25.4 mm diameter) were used to detect the start and stop signals of the experiments. While a more detailed description of the PALS system has been provided elsewhere,[43,44] a photograph of the setup along with a schematic illustration is presented in Figure 2.

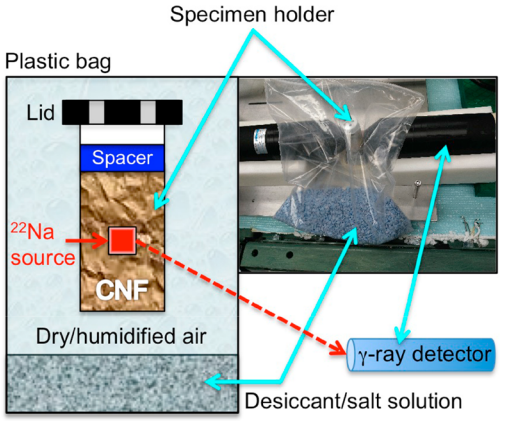

Figure 2. Schematic illustration of the PALS setup employed in this study. A sealed plastic bag contains a glass vial (into which is placed a TO-CNF specimen and the ^{22}Na positron source) and a desiccant or salt solution to maintain a specific RH level within an enclosed plastic bag.

Specimens to be examined were prepared by breaking about eight films into pieces (totaling ~1.6 g) that were subsequently inserted into a vial. The positron source was positioned among the sample pieces, which were pressed to minimize spurious signals from air, and the vial was capped. Multiple holes were drilled into the cap of each vial to allow equilibration with the surrounding environment. Sample-filled vials were placed in plastic bags containing either desiccants or ~150 mL of a suitable salt solution to generate the RH levels listed in Table 2. The plastic bags were then sealed, and the samples were allowed to equilibrate. The desiccant remained blue at 0% RH, ensuring that the sample environment was at 0% RH (otherwise the desiccant would turn red). To monitor/confirm the equilibration process, PALS spectra, recording at least 1.5 × 10^6 events, were acquired at ambient temperature every 1–2 days. Resultant spectra were primarily fitted with three annihilation lifetimes using the POSFIT software package, and the regressed value of τ_3 was related to the size of free-volume elements via a shape-free quantum-mechanical model.[40]

Table 2. Relative Humidity Levels Achieved in the PALS Analyses[a]

water-vapor source	RH levels (%)
desiccant	0
saturated $MgCl_2$	33 ± 0.2
saturated $Mg(NO_3)_2$	53 ± 0.2
saturated NaCl	75 ± 0.1
deionized water	100

[a]Reported RH levels are extracted from ref 6, and the error corresponds to the standard deviation.

RESULTS AND DISCUSSION

TO-CNF Film Characterization. Conductiometric titration reveals that the carboxylic acid content [−COO− + COOH] of the TO-CNF generated here is 1343 ± 7.2 μmol/g. Acid hydrolysis confirms that the cellulose content is ~79 wt %, whereas the acid-soluble lignin is ~0.6 wt % (with no detectable acid-insoluble lignin). Galacto-(glucomannan) and xylan account for ~9 and ~7 wt %, respectively. Films fabricated from the procedure described here measure ~20 μm thick and appear highly transparent, as generally evidenced by the photographs presented in Figure 3. While the films appear visually similar when cast from sonicated or nonsonicated suspensions, their appearance is noticeably affected by the drying temperature. Films dried at ambient temperature for about 23 days are virtually defect-free (Figure 3A). Films dried at 35 °C over the course of 6 days display visible bubbles (Figure 3C), and those dried at 50 °C for 1–2 days exhibit a large population of bubbles (Figure 3E). This observation clearly indicates that, as the specimens are subjected to higher temperatures and expedited film drying, the resulting TO-CNF films more readily entrap liquid water, which produces bubbles upon vaporization. This observation is consistent with SEM images of cross-fractured films, displayed in Figure 3. An increase in the drying temperature and corresponding rate of film formation is accompanied by enhanced film densification in regions away from bubbles. The mechanical strength of the films is likewise sensitive to bubble formation (and, hence, drying time), since films dried quickly are fragile and tear easily. The specimens displayed in Figure 3B, D, and F are all sonicated to permit discrimination by SEM (this is not required at the length scale associated with visual examination). According to the DLS results provided in Figure 4, sonication

DOI: 10.1021/acs.biomac.7b01814
Biomacromolecules XXXX, XXX, XXX−XXX

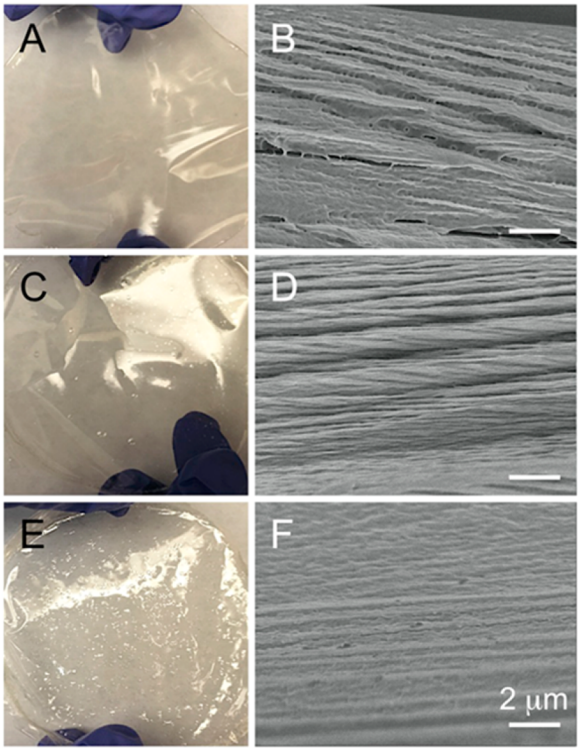

Figure 3. Photographs (left) and cross-sectional SEM images (right) of sonicated TO-CNF films dried at different temperatures: (A, B) ambient temperature, (C, D) 35 °C, and (E, F) 50 °C.

serves to reduce the mean TO-CNF length and shift the size distribution to shorter nanofibrils.

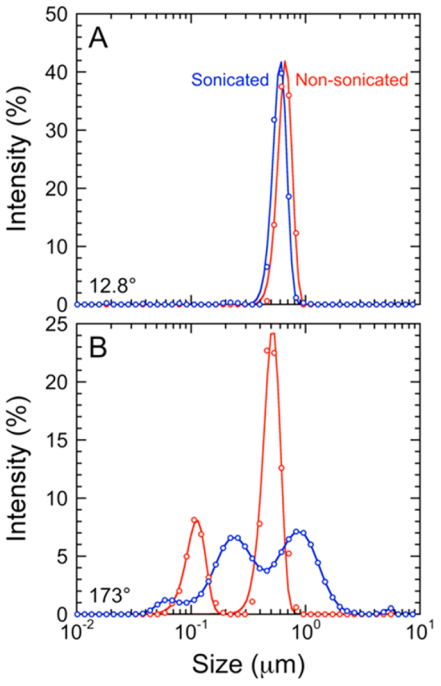

Figure 4. Nanofibril dimensions obtained from DLS at (A) 12.8° and (B) 173° on TO-CNF suspensions with (blue) and without (red) sonication. The solid lines represent Gaussian fits to the peaks in the data.

TO-CNF Film Swelling. Swelling tests performed in a Percival climate chamber on four replicates establish that S lies between ~24−33% after exposure to 90 ± 2% RH and 23.9 °C for 96 h. Figure 5A displays the time dependence of S for films

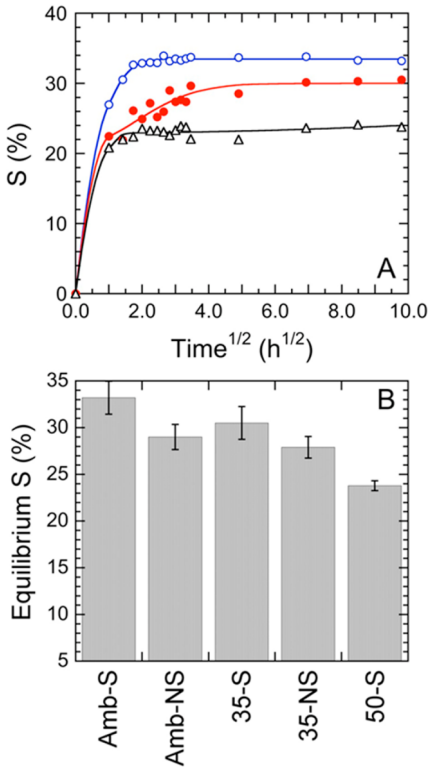

Figure 5. (A) Time-dependent swelling (S) curves determined from eq 5 at 90% RH for TO-CNF films prepared by sonication and dried at three different temperatures: ambient (○), 35 °C (●), and 50 °C (△). The solid lines are regressions of eq 1 to the data, and the error bars denote standard errors. (B) Equilibrium S values obtained from swelling curves at 90% RH for the five different specimen designations examined in this study (cf. Table 1).

that have been sonicated as suspensions and dried at three different temperatures. Application of eq 1 to these data results in the following values of α_1 and α_2, respectively (in h): 0.036 and 1.177 (ambient temperature), 0.008 and 6.553 (35 °C), and 0.430 and 9.341 × 10^4 (50 °C). After exposure to water vapor for 1 h, the TO-CNF films dried at ambient temperature swell by 27%, whereas those dried at 35 and 50 °C swell to 22 and 21%, respectively. After 12/24 h, these S levels increase to 34/34% (ambient), 30/29% (35 °C), and 22/22% (50 °C). Corresponding values of S at 96 h are 33, 31, and 24%, respectively, revealing that swelling is negligible after 12 h. In fact, these results indicate that at least ~70% of the equilibrium swelling in these TO-CNF films occurs within the first hour of exposure. In addition, the swelling results displayed in Figure 5A likewise demonstrate that an increase in drying temperature promotes a reduction in equilibrium swelling. This specimen preparation issue, as well as suspension sonication, is explicitly addressed in Figure 5B, which shows that, while sonication tends to improve swelling modestly (by 14% at ambient temperature and 9% at 35 °C), increased drying time lowers swelling to a greater extent (by 28% from ambient temperature to 50 °C). This latter observation, which is consistent with the SEM images provided in Figure 3, implies that densified TO-

DOI: 10.1021/acs.biomac.7b01814
Biomacromolecules XXXX, XXX, XXX−XXX

Table 3. PALS Lifetimes Measured at 0% RH for TO-CNF Films Prepared from Sonicated and Nonsonicated Suspensions

specimen	τ_1 (ns)	I_1 (%)	τ_2 (ns)	I_2 (%)	τ_3 (ns)	I_3 (%)	τ_4 (ns)	I_4 (%)
Three-Lifetime Fitting								
Amb-NS	0.11 ± 0.05	11.81 ± 5.54	0.38 ± 0.01	73.28 ± 5.34	1.27 ± 0.01	14.91 ± 0.32		
Amb-S	0.19 ± 0.02	17.83 ± 2.14	0.40 ± 0.01	68.19 ± 1.99	1.36 ± 0.01	13.98 ± 0.21		
Four-Lifetime Fitting								
Amb-NS	0.08 ± 0.01	14.28 ± 1.03	0.37 ± 0.01	70.43 ± 0.84	1.24 ± 0.02	15.18 ± 0.32	7.47 ± 5.76	0.11 ± 0.04
Amb-S	0.09 ± 0.01	16.01 ± 1.81	0.37 ± 0.01	67.88 ± 1.62	1.19 ± 0.04	15.11 ± 0.34	2.55 ± 0.46	1.01 ± 0.58

CNF films dried at elevated temperatures are more likely to hinder the sorption of water molecules and thus swell. Another important consideration here is that hornification might be at least partially responsible for this apparent result. Hornification, an irreversible stiffening of cellulosic chains that naturally occurs upon drying as glucose units undergo chemical cross-linking,[45] would also serve to inhibit swelling. This process has been reported to increase with increasing carboxylate content[46] and drying temperature.[47]

Free Volume: Dry TO-CNF Films. In this section, we explore the effects of sonication and drying temperature on the free volume of dry TO-CNF films. To begin, PALS spectra collected from films at 0% RH prepared from both sonicated and nonsonicated suspensions dried at ambient temperature have been well-fitted with three (and, for comparison, four) characteristic lifetimes in eq 2. Multiple spectra have been acquired to confirm that the specimens have reached their equilibrium state, and results from the last series are listed as typical values in Table 3. The regressed value of the o-Ps lifetime (τ_3) ascertained from the sonicated specimen after regression with three characteristic lifetimes (1.36 ns) is noticeably larger than that of the nonsonicated one (1.27 ns), which suggests that the sonication process affects the radius (r) of the free-volume pores. Calculated values of r—0.206 ± 0.002 and 0.218 ± 0.001 nm for the Amb-NS and Amb-S specimens, respectively—are lower than results previously reported[24] for dry TO-CNF films (r = 0.235 nm). Corresponding values of L from eq 4 are (5.26 ± 0.08) × 10^{-3} nm^3 (Amb-NS) and (5.78 ± 0.06) × 10^{-3} nm^3 (Amb-S), indicating that the sonicated specimen possesses more free volume (with modestly larger free-volume pores). This result might help to explain the sonication-induced increase in equilibrium swelling evident in Figure 5B. To discern the extent to which the values of τ_3 and L are robust, the PALS spectra have also been fitted to four characteristic lifetimes (cf. Table 3). While τ_4 and I_4 are also metrics of free volume in polymeric media and suggest the presence of larger free-volume pores, the values of I_4 are substantially smaller than the other intensity values (~1% for the sonicated specimen and ~0.1% for the nonsonicated one), in which case these contributions to the free-volume analysis are probably negligible and are not considered further in this work. Another indicator that these additional lifetimes are most likely inconsequential is the surprisingly large uncertainty in τ_4 relative to all the other extracted τ_j values in Table 3 (<0.05 ns).

In addition to TO-CNF suspension sonication, another consideration of importance in this section is the drying temperature. Three-lifetime analysis of relevant PALS spectra as above for only the sonicated specimens yields free-volume pore radii of 0.215 ± 0.001 and 0.212 ± 0.001 nm at drying temperatures of 35 and 50 °C, respectively. Values of r and L extracted from these data are displayed as a function of drying temperature (where ambient is taken as 21 °C) in Figure 6 and reveal that, while r systematically decreases, L decreases to a plateau, with increasing drying temperature. That is, increasing the drying temperature from 35 to 50 °C has no discernible effect on L. These changes in free-volume characteristics with drying temperature can be explained in terms of the hierarchical structure of TO-CNF.[6] We have established that an increase in drying temperature promotes film densification, as independently determined from SEM (Figure 3) and equilibrium swelling (Figure 5). On the basis of these experimental observations, such drying-induced densification is presumed to influence nanofibrillar packing. If this is the case, then it follows that either interfibrillar pores or possibly the nanofibrils themselves are most likely compressed.

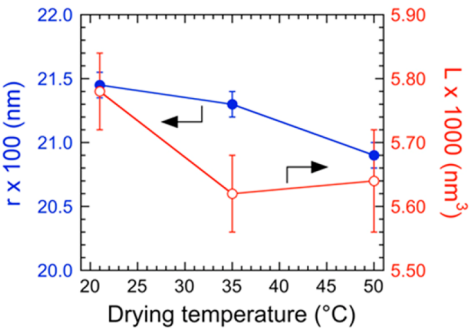

Figure 6. Free-volume pore radius (r) and total free volume (L) calculated from PALS spectra collected from TO-CNF films that were sonicated as suspensions and dried at different temperatures (color-coded). The solid lines serve to connect the data, and the error bars denote standard errors.

Since the crystalline regions of the chains are expected to remain largely unaffected, intrachain, as well as interchain, amorphous regions responsible for the free volume within CNF densify at the nanoscale, resulting in smaller free-volume pores. Faster drying times at elevated temperatures most likely prevents the chains from adopting their lowest energy conformations, and thus, the population of free-volume pores increases (apparently to a limit) at higher drying temperatures. Corresponding values of I_3 under these conditions are calculated to be (14.0 ± 0.2)% for Amb-S and (14.8 ± 0.4)% for 50-S.

We anticipate that not all of the free-volume pores in this scenario are accessible to penetrant water molecules, in which case equilibrium swelling decreases. In marked contrast, sonication loosens the nanofibrils[48] and disrupts their crystalline regions[49] prior to drying. Doing so simultaneously increases both r and L, as reported above.

Free Volume: Swollen TO-CNF Films. Thus far, we have explored the effects of suspension sonication and drying temperature on the free-volume and swelling characteristics of TO-CNF films at 0% RH. In this section, the response of TO-CNF films exposed to sonication and dried at ambient temperature (designated as Amb-S in Table 1) is monitored at several different RH levels. The tests performed here utilize

DOI: 10.1021/acs.biomac.7b01814
Biomacromolecules XXXX, XXX, XXX−XXX

the setup described with regard to Figure 2. Compared to the static swelling performed in the climate chamber (cf. Figure 5), the films investigated by PALS require significantly longer equilibration times (several days vs ∼12 h) due to the experimental configuration. Representative peak-normalized PALS spectra obtained from Amb-S specimens at different RH levels and ambient temperature after an exposure time of 5−11 days (spectra shown correspond to equilibrium conditions at each RH level) are presented in Figure 7 and

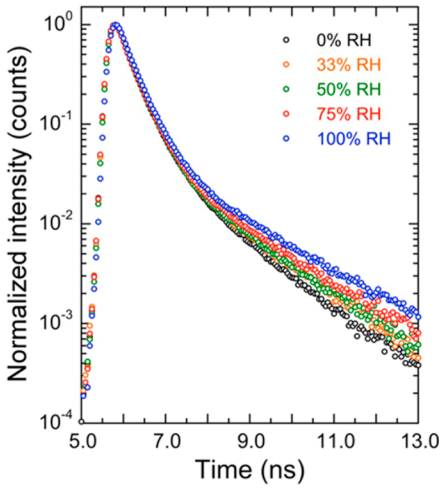

Figure 7. Peak-normalized PALS spectra collected from TO-CNF films prepared from sonicated aqueous TO-CNF suspensions dried at ambient temperature for 23 days and measured at different RH levels (see legend) at ambient temperature.

qualitatively indicate that the o-Ps lifetimes are systematically shifted to higher values as the RH level is increased. Corresponding values of r and I_3 extracted by analyzing such spectra according to eq 2 and the model provided elsewhere[40] with three characteristic lifetimes are provided in Figure 8 and

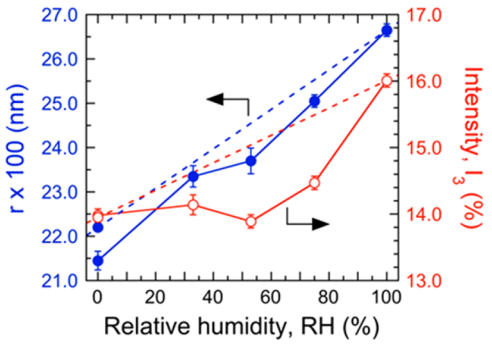

Figure 8. Long-time values of r (blue) and I_3 (red) as functions of relative humidity (RH) at ambient temperature (color-coded). The solid lines serve to connect the data in the increasing RH direction, the dashed lines connect the data upon redrying, and the error bars denote standard errors.

reveal that r (which exhibits the same RH dependence as τ_3, not included for that reason) increases monotonically with increasing RH level from 0.215 ± 0.001 nm at 0% to 0.267 ± 0.001 nm at 100%, an increase of about 24%. The dependence of I_3 on RH differs slightly: it remains relatively constant up to 53% RH and then increases by about 15%. To discern the extent of hysteresis upon deswelling, the specimen at 100% RH was redried to 0% RH and remeasured. As seen in Figure 8, the initial free-volume intensity is recovered, but the free-volume pore size is not. The original pore radius measures 0.215 nm, while the radius after redrying is 0.222 nm. At macroscopic length scales, pulp drying results in lower porosity.[45,50] Free volume that exists at nanoscopic length scales is not, however, affected by surface tension in the same way as macropores when water evaporates.

To determine the time dependence of RH-induced free-volume changes, we have performed PALS at different times at each RH level to follow the evolution of free-volume pore size and o-Ps intensity during the course of the experiment. The results are shown for both r and I_3 in Figure 9 and generally

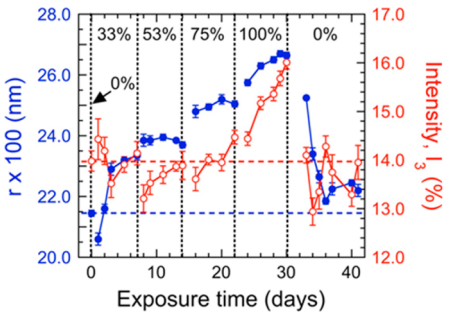

Figure 9. Free-volume pore radius and intensity of the Amb-S specimen in the presence of different RH levels (labeled) as a function of exposure time. Dotted lines represent the times at which the long-time value is recorded for a given RH level (these values are displayed in Figure 8).

demonstrate that, except during the initial swelling and final redrying, r is not as sensitive to exposure time at each RH as I_3. An interesting observation on the first day at 33% RH provides evidence of atypical pore filling, which is also identified in other polymer systems.[51] This phenomenon is manifested as a slight, yet statistically significant, initial decrease in average pore radius from 0.215 to 0.206 nm (a reduction of ∼4%) before r increases or levels off at longer times. Values of r and I_3 recorded at the longest time examined at each RH level are presumed to be representative of near-equilibrium and are used to construct Figure 8. While r behaves nearly as anticipated (even during the transient periods of initial swelling and final redrying), the free-volume intensity does not during the transient periods. Upon initial swelling, for instance, I_3 decreases over the course of the first 3 days as r systematically increases. As the specimen is redried, r expectedly decreases to a relatively constant value. While we do not have a conclusive explanation for these results, we posit that the presence of water molecules might be a contributing factor. Free water possesses an o-Ps lifetime of 1.86 ns,[52] which might impact the measured free-volume characteristics here if water in the TO-CNF film elicits its own o-Ps signal. Free water molecules can potentially contribute to the extracted values of r, since its own "free-volume" (Ps bubble) radius is 0.27 nm (cf. Table 4),[52] which is comparable to the pore size ascertained here and in cellulose acetate.[25] Below, we address the issue of how water contributes to PALS spectra at different RH levels.

The Kelvin equation describes the thermodynamics governing pore filling and assumes that pores <10 nm are not filled at 90% RH under ambient conditions. While this relationship can elucidate the size distribution of pores through the use of adsorption porosimetry, it is only valid for relatively large pores

DOI: 10.1021/acs.biomac.7b01814
Biomacromolecules XXXX, XXX, XXX−XXX

Table 4. o-Ps Characteristics and Pore Radii for Dry TO-CNF Film Dried from Sonicated Suspension and Pure Water

system	τ_3 (ns)	I_3 (%)	r (nm)
TO-CNF film	1.36 ± 0.01	13.98 ± 0.21	0.215 (this work)
pure water[52]	1.86	26.9 ± 0.5	0.27

and does not account for site-specific interactions such as hydrogen bonding in its surface tension term. It nonetheless provides an experimental tactic, as detailed in the following section. Our results reported here, as well as others,[25,51] indicate that water initially fills free-volume pores measuring ≪10 nm. The PALS results provided in Figure 8 establish that the o-Ps intensity is relatively constant, whereas r systematically increases, up to ∼53% RH, implying that the free-volume pores expand in this interval but that their number density does not change appreciably. Since evidence of pore filling is observed after just 1 d at 33% RH in Figure 9, water molecules most likely adsorb to the surface of the free-volume pores and partially fill them. Pore filling is subsequently overtaken by concomitant pore swelling, which serves to push neighboring TO-CNF chains away from each other. Since these water molecules are bound by hydrogen bonds, they should not be treated as free water with the free-volume characteristics listed in Table 4. At RH levels beyond 53%, both free-volume pore size and intensity increase with increasing exposure time in Figure 8. This observation is explained by water opening the amorphous regions of TO-CNF, thus creating more and larger free-volume pores. Under these conditions, however, the existence of free water can generate a PALS signal with the o-Ps intensity and pore size included in Table 4. As seen in Figure 3B, the TO-CNF films exhibit interfibrillar pores that measure in the micrometer range. While these are not to be confused with the free-volume pores, they could be filled with free water at high RH levels, thereby eliciting a pure water signal in PALS. This possibility is supported by oxygen permeability data,[24] which increases as TO-CNF films are exposed to water vapor, signifying that water penetrates into interfibrillar spaces and thus reduces film density.

To further determine the role of water in the PALS analysis, the o-Ps intensity data in Figure 8 have been correlated with RH level by an empirical exponential function to interpolate the o-Ps intensity at 90% RH. With a regression coefficient (R^2) of 0.98, this correlation yields an intensity of 15.1%, which can be used to ascertain if I_3 corresponds to the mass-weighted average of o-Ps intensities from free water and cellulose. The swelling data included in Figure 5A indicate that the mean equilibrium swelling for Amb-S at 90% RH is 33.2 ± 1.8%, which is equivalent to 24.9 ± 1.0 wt % water relative to the total swollen mass. To test the hypothesis above, the total signal intensity is expressed in terms of the pure water intensity (I_{3w}), the contributing water fraction (f_w), the TO-CNF intensity (I_{3c}), and the contributing cellulose fraction (f_c) in a linear fashion to yield

$$I_3 = f_w I_{3w} + f_c I_{3c} \quad (6)$$

By utilizing the values listed in Table 5, it becomes clear that not all of the free water contributes to the measured o-Ps signal, since this leads to a higher value of I_3 than interpolated from measurements (∼17% > ∼15%). Solving eq 6 for f_w with the requirement that $f_w + f_c = 1$ and $I_3 = 0.151$ yields 8.7 wt % water, thereby verifying that a nontrivial fraction of water in the system is bound to the TO-CNF chains and incapable of contributing an o-Ps signal to PALS spectra. A similar comparison performed by applying a simple linear rule of mixtures to the o-Ps lifetimes for pure water and cellulose results in 7.9 wt % water, which is in fair agreement with the water content from the o-Ps intensity calculations.

The free water fractions calculated above from the o-Ps intensities of the pure and swollen TO-CNF systems reveals that 35% of the water in the Amb-S specimen is free (and contributes to the measured value of I_3) and the remaining 65% is bound to the cellulose and is responsible for the measured free-volume characteristics of the nanofibrils. A related issue to consider is the possibility that bound water alters the formation of o-Ps in such a fashion that a reduction in o-Ps intensity due to the presence of water-containing free-volume pores is compensated by the intensity contribution from free water. For this effect to be realized, the correct o-Ps intensities and characteristic lifetimes would have to be concurrently maintained over the entire RH range, which is not very likely. On the basis of the experimental results reported here, water initially fills existing free-volume pores (as evidenced by a decrease in r after 1 day in Figure 9) but is strongly bound to the cellulose (without contributing to the o-Ps intensity) in general agreement with the classification of "nonfreezing" water during initial cellulose swelling.[53,54] After the initial pore size reduction, water at longer exposure times and higher RH levels expands the existing free volume pores. In this regime, the o-Ps intensity remains relatively steady, suggesting that most of the water remains tightly bound to the cellulose without contributing to the o-Ps intensity and consists of both "nonfreezing" and "freezing bound" water.[54] The latter consists of water molecules that are tightly bound to cellulose and exhibit a significantly depressed freezing point compared to free water. At RH levels above ∼53% RH, however, the presence of free water becomes non-negligible. Since the concurrent increases in o-Ps characteristic lifetime (which follows the RH dependence of r) and intensity in Figure 9 are much more pronounced than those attributable to free water, we propose that bonded water opens new free-volume pores in amorphous interchain regions in addition to swelling existing pores. A schematic illustration of these free-volume changes is depicted in Figure 10.

CONCLUSIONS

In this study, we have investigated the macroscopic swelling and accompanying free-volume changes of TO-CNF films. While these films swell according to expectation when subjected to 90% RH water vapor, swelling is reduced when the film drying temperature is increased. This observation is attributed to higher film density, as verified by SEM and

Table 5. Weighted PALS Intensities of Water and TO-CNF Films Swollen at 90% RH

equilibrium swelling (%)	f_w	$f_w \times I_{3w}$	$f_c \times I_{3c}$	I_3 (%) from eq 6
31.4	0.239	0.239 × 26.9 = 6.43	0.761 × 13.98 = 10.64	17.07 ± 0.2
35.0	0.259	0.259 × 26.9 = 6.97	0.741 × 13.98 = 10.36	17.33 ± 0.2

DOI: 10.1021/acs.biomac.7b01814
Biomacromolecules XXXX, XXX, XXX−XXX

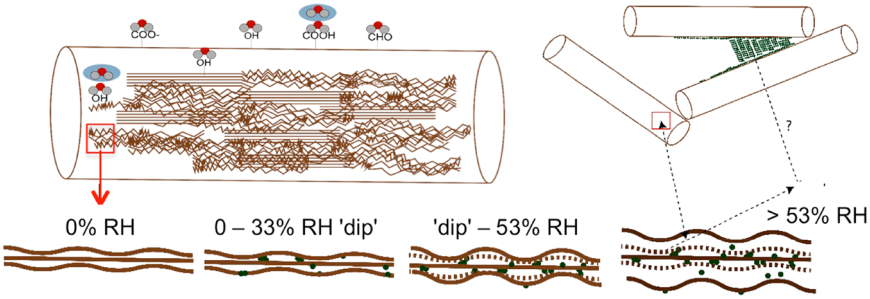

Figure 10. Proposed model for water–cellulose interactions in the amorphous regions of cellulose chains within CNF (rod). During the initial transient swelling between 0 and ~33% RH, water fills intra/interchain free-volume pores and reduces the measured free volume. Beyond this transient and up to ~53% RH, the free-volume pores expand without the creation of new pores. Beyond ~53% RH, water generates the formation of new pores by displacing chains, thus leading to simultaneous increases in o-Ps intensity and pore radius.

suggesting enhanced hornification. In marked contrast, the total free volume of fully dried films is not affected by the drying temperature even though the pore size decreases and the pore number density increases with increasing drying temperature. Suspension sonication prior to casting serves to increase the free-volume pore size due to a combination of disruption and size reduction of the TO-CNF fibrils. Subjecting TO-CNF films to various RH levels reveals free-volume pore filling at low levels (<33% RH). As the RH is increased, free-volume pores expand. At RH levels beyond ~53%, water likely creates new free-volume pores and behaves as free water inside the film, thereby eliciting a free-water PALS signal. This conclusion is supported by comparing PALS spectra with free-volume intensity and lifetime calculations. Lastly, swollen films that are subjected to redrying exhibit slight free-volume pore size hysteresis. This study establishes a direct relationship between macroscale and nanoscale water sorption in TO-CNF films prepared under several different conditions.

AUTHOR INFORMATION

Corresponding Authors

*E-mail: rich_spontak@ncsu.edu. Phone: +1 919 515 4200.
*E-mail: oyvind.w.gregersen@ntnu.no. Phone: +47 73 594 029.

ORCID

Richard J. Spontak: 0000-0001-8458-0038

Notes

The authors declare no competing financial interest.

ACKNOWLEDGMENTS

This project was financially supported by a NANO 2021 project and the NANO-MBE project (No. 239172) sponsored by the Research Council of Norway. S.-A.J. is grateful to the Eastman Chemical Center of Excellence for funding. We thank Ms. I. Leirset and Ms. A. Reitan for technical assistance and Dr. J. Chiera for access to the Percival climate cabinet. We are immensely grateful to Södra for providing the softwood pulp.

REFERENCES

(1) Saito, T.; Nishiyama, Y.; Putaux, J. L.; Vignon, M.; Isogai, A. Homogeneous Suspensions of Individualized Microfibrils from TEMPO-Catalyzed Oxidation of Native Cellulose. *Biomacromolecules* **2006**, *7*, 1687–1691.

(2) Ottesen, V.; Syverud, K.; Gregersen, Ø. W. Mixing of Cellulose Nanofibrils and Individual Furnish Components: Effects on Paper Properties and Structure. *Nord. Pulp Pap. Res. J.* **2016**, *31*, 441–447.

(3) Alexandrescu, L.; Syverud, K.; Nicosia, A.; Santachiara, G. Airborne Nanoparticles Filtration by Means of Cellulose Nanofibril Based Materials. *J. Biomater. Nanobiotechnol.* **2016**, *07*, 29–36.

(4) Rashad, A.; Mustafa, K.; Heggset, E. B.; Syverud, K. Cytocompatibility of Wood-Derived Cellulose Nanofibril Hydrogels with Different Surface Chemistry. *Biomacromolecules* **2017**, *18*, 1238–1248.

(5) Bulota, M.; Tanpichai, S.; Hughes, M.; Eichhorn, S. J. Micromechanics of TEMPO-Oxidized Fibrillated Cellulose Composites. *ACS Appl. Mater. Interfaces* **2012**, *4*, 331–337.

(6) Dufresne, A. *Nanocellulose: From Nature to High Performance Tailored Materials*; Walter de Gruyter GmbH: Berlin, 2012.

(7) Isogai, A.; Saito, T.; Fukuzumi, H. TEMPO-Oxidized Cellulose Nanofibers. *Nanoscale* **2011**, *3*, 71–85.

(8) Rodionova, G.; Saito, T.; Lenes, M.; Eriksen, Ø.; Gregersen, Ø.; Kuramae, R.; Isogai, A. TEMPO-Mediated Oxidation of Norway Spruce and Eucalyptus Pulps: Preparation and Characterization of Nanofibers and Nanofiber Dispersions. *J. Polym. Environ.* **2013**, *21*, 207–214.

(9) Jiang, F.; Hsieh, Y. L. Chemically and Mechanically Isolated Nanocellulose and Their Self-Assembled Structures. *Carbohydr. Polym.* **2013**, *95*, 32–40.

(10) Saito, T.; Kimura, S.; Nishiyama, Y.; Isogai, A. Cellulose Nanofibers Prepared by TEMPO-Mediated Oxidation of Native Cellulose. *Biomacromolecules* **2007**, *8* (8), 2485–2491.

(11) Ishii, D.; Saito, T.; Isogai, A. Viscoelastic Evaluation of Average Length of Cellulose Nanofibers Prepared by TEMPO-Mediated Oxidation. *Biomacromolecules* **2011**, *12*, 548–550.

(12) Yuan, X.; Cheng, G. From Cellulose Fibrils to Single Chains: Understanding Cellulose Dissolution in Ionic Liquids. *Phys. Chem. Chem. Phys.* **2015**, *17*, 31592–31607.

(13) Sèbe, G.; Ham-Pichavant, F.; Ibarboure, E.; Koffi, A. L. C.; Tingaut, P. Supramolecular Structure Characterization of Cellulose II Nanowhiskers Produced by Acid Hydrolysis of Cellulose I Substrates. *Biomacromolecules* **2012**, *13*, 570–578.

(14) Syverud, K.; Chinga-Carrasco, G.; Toledo, J.; Toledo, P. G. A Comparative Study of Eucalyptus and Pinus Radiata Pulp Fibres as Raw Materials for Production of Cellulose Nanofibrils. *Carbohydr. Polym.* **2011**, *84*, 1033–1038.

(15) Chinga-Carrasco, G.; Yu, Y.; Diserud, O. Quantitative Electron Microscopy of Cellulose Nanofibril Structures from Eucalyptus and Pinus Radiata Kraft Pulp Fibers. *Microsc. Microanal.* **2011**, *17*, 563–571.

(16) White, R. P.; Lipson, J. E. G. Polymer Free Volume and Its Connection to the Glass Transition. *Macromolecules* **2016**, *49*, 3987–4007.

(17) Jean, Y. C.; Van Horn, J. D.; Hung, W.-S.; Lee, K.-R. Perspective of Positron Annihilation Spectroscopy in Polymers. *Macromolecules* **2013**, *46*, 7133–7145.

(18) Dudowicz, J.; Freed, K. F.; Douglas, J. F. In *Advances in Chemical Physics*, 1st ed.; Rice, S. A., Ed.; John Wiley & Sons, Inc.: Hoboken, NJ, 2008; pp 125–222.

DOI: 10.1021/acs.biomac.7b01814
Biomacromolecules XXXX, XXX, XXX–XXX

(19) Simha, R.; Somcynsky, T. On the Statistical Thermodynamics of Spherical and Chain Molecule Fluids. *Macromolecules* **1969**, *2*, 342−350.
(20) Nakanishi, H.; Jean, Y. C.; Smith, E. G.; Sandreczki, T. C. Positronium Formation at Free-Volume Sites in the Amorphous Regions of Semicrystalline PEEK. *J. Polym. Sci., Part B: Polym. Phys.* **1989**, *27*, 1419−1424.
(21) Merkel, T. C.; Freeman, B. D.; Spontak, R. J.; He, Z.; Pinnau, I.; Meakin, P.; Hill, A. J. Ultrapermeable, Reverse-Selective Nanocomposite Membranes. *Science* **2002**, *296*, 519.
(22) Nagel, C.; Gu, K.; Fritsch, D.; Strunskus, T.; Faupel, F. Free Volume and Transport Properties in Highly Selective Polymer Membranes. *Macromolecules* **2002**, *35*, 2071−2077.
(23) Shantarovich, V. P.; Kevdina, I. B.; Yampolskii, Y. P.; Alentiev, A. Y. Positron Annihilation Lifetime Study of High and Low Free Volume Glassy Polymers: Effects of Free Volume Sizes on the Permeability and Permselectivity. *Macromolecules* **2000**, *33*, 7453−7466.
(24) Fukuzumi, H.; Saito, T.; Iwamoto, S.; Kumamoto, Y.; Ohdaira, T.; Suzuki, R.; Isogai, A. Pore Size Determination of TEMPO-Oxidized Cellulose Nanofibril Films by Positron Annihilation Lifetime Spectroscopy. *Biomacromolecules* **2011**, *12*, 4057−4062.
(25) Chen, G. Q.; Kanehashi, S.; Doherty, C. M.; Hill, A. J.; Kentish, S. E. Water Vapor Permeation through Cellulose Acetate Membranes and Its Impact upon Membrane Separation Performance for Natural Gas Purification. *J. Membr. Sci.* **2015**, *487*, 249−255.
(26) Hodge, R. M.; Bastow, T. J.; Edward, G. H.; Simon, G. P.; Hill, A. J. Free Volume and the Mechanism of Plasticization in Water-Swollen Poly(vinyl Alcohol). *Macromolecules* **1996**, *29*, 8137−8143.
(27) Madani, M. M.; Miron, R. R.; Granata, R. D. PALS Free Volume Study of Dry and Water Saturated Epoxies. *J. Coat. Technol.* **1997**, *69*, 45−54.
(28) Soles, C. L.; Chang, F. T.; Gidley, D. W.; Yee, A. F. Contributions of the Nanovoid Structure to the Kinetics of Moisture Transport in Epoxy Resins. *J. Polym. Sci., Part B: Polym. Phys.* **2000**, *38*, 776−791.
(29) Morrison, J. L.; Dzieciuch, M. A. The Thermodynamic Properties of the System Cellulose − Water Vapor. *Can. J. Chem.* **1959**, *37*, 1379−1390.
(30) Belbekhouche, S.; Bras, J.; Siqueira, G.; Chappey, C.; Lebrun, L.; Khelifi, B.; Marais, S.; Dufresne, A. Water Sorption Behavior and Gas Barrier Properties of Cellulose Whiskers and Microfibrils Films. *Carbohydr. Polym.* **2011**, *83*, 1740−1748.
(31) Svagan, A. J.; Hedenqvist, M. S.; Berglund, L. Reduced Water Vapour Sorption in Cellulose Nanocomposites with Starch Matrix. *Compos. Sci. Technol.* **2009**, *69*, 500−506.
(32) Wahba, M.; Nashed, S. Moisture Relations of Cellulose. III. Sorption Hysteresis and the Effect of Temperature. *J. Text. Inst. Trans.* **1957**, *48*, T1−T20.
(33) Okubayashi, S.; Griesser, U. J.; Bechtold, T. A Kinetic Study of Moisture Sorption and Desorption on Lyocell Fibers. *Carbohydr. Polym.* **2004**, *58*, 293−299.
(34) Howsmon, J. A. Water Sorption and the Poly-Phase Structure of Cellulose Fibers. *Text. Res. J.* **1949**, *19*, 152−162.
(35) Kohler, R.; Alex, R.; Brielmann, R.; Ausperger, B. A New Kinetic Model for Water Sorption Isotherms of Cellulosic Materials. *Macromol. Symp.* **2006**, *244*, 89−96.
(36) Kohler, R.; Dück, R.; Ausperger, B.; Alex, R. A Numeric Model for the Kinetics of Water Vapor Sorption on Cellulosic Reinforcement Fibers. *Compos. Interfaces* **2003**, *10*, 255−276.
(37) Tao, S. J. Positronium Annihilation in Molecular Substances. *J. Chem. Phys.* **1972**, *56*, 5499−5510.
(38) Eldrup, M.; Lightbody, D.; Sherwood, J. N. The Temperature Dependence of Positron Lifetimes in Solid Pivalic Acid. *Chem. Phys.* **1981**, *63*, 51−58.
(39) Goworek, T.; Jasińska, B.; Wawryszczuk, J.; Zaleski, R.; Suzuki, T. On Possible Deviations of Experimental PALS Data from Positronium Pick-off Model Estimates. *Chem. Phys.* **2002**, *280*, 295−307.
(40) Wada, K.; Hyodo, T. A Simple Shape-Free Model for Pore-Size Estimation with Positron Annihilation Lifetime Spectroscopy. *J. Phys. Conf. Ser.* **2013**, *443*, 012003.
(41) Sousa, A.; Souza, K. C.; Reis, S. C.; Sousa, R. G.; Windmöller, D.; Machado, J. C.; Sousa, E. M. B. Positron Annihilation Study of Pore Size in Ordered SBA-15. *J. Non-Cryst. Solids* **2008**, *354*, 4800−4805.
(42) Saito, T.; Isogai, A. TEMPO-Mediated Oxidation of Native Cellulose. The Effect of Oxidation Conditions on Chemical and Crystal Structures of the Water-Insoluble Fractions. *Biomacromolecules* **2004**, *5*, 1983−1989.
(43) Liu, M.; Hawari, A. I. Positron Characterization of Neutron Irradiated Reactor-Grade Graphite. *Trans. Am. Nucl. Soc.* **2014**, *110*, 970−972.
(44) Gidley, D. W.; Peng, H.-G.; Vallery, R. S. Annihiliation as a Method to Characterize Porous Materials. *Annu. Rev. Mater. Res.* **2006**, *36*, 49−79.
(45) Fernandes Diniz, J. M. B.; Gil, M. H.; Castro, J. A. A. M. Hornification − Its Origin and Interpretation in Wood Pulps. *Wood Sci. Technol.* **2004**, *37*, 489−494.
(46) Racz, I.; Borsa, J. Swelling of Carboxymethylated Cellulose Fibres. *Cellulose* **1997**, *4*, 293−303.
(47) Kato, K. L.; Cameron, R. E. A Review of the Relationship between Thermally-Accelerated Ageing of Paper and Hornification. *Cellulose* **1999**, *6*, 23−40.
(48) Saito, T.; Kuramae, R.; Wohlert, J.; Berglund, L. A.; Isogai, A. An Ultrastrong Nanofibrillar Biomaterial: The Strength of Single Cellulose Nanofibrils Revealed via Sonication-Induced Fragmentation. *Biomacromolecules* **2013**, *14*, 248−253.
(49) Sumari, S.; Roesyadi, A.; Sumarno, S. Effects of Ultrasound on the Morphology, Particle Size, Crystallinity, and Crystallite Size of Cellulose. *Ind. Aliment. Sci. Study Res. Chem. Chem. Eng. Biotechnol.* **2013**, *14*, 229−239.
(50) Stone, J. E.; Scallan, A. M. A Structural Model for the Cell Wall of Water-Swollen Wood Pulpfibres Based on Their Accessibility to Macromolecules. *Cellul. Chem. Technol.* **1968**, *2*, 343−358.
(51) Muramatsu, M.; Okura, M.; Kuboyama, K.; Ougizawa, T.; Yamamoto, T.; Nishihara, Y.; Saito, Y.; Ito, K.; Hirata, K.; Kobayashi, Y. Oxygen Permeability and Free Volume Hole Size in Ethylene-Vinyl Alcohol Copolymer Film: Temperature and Humidity Dependence. *Radiat. Phys. Chem.* **2003**, *68*, 561−564.
(52) Eldrup, M. Positron Lifetimes in Pure and Doped Ice and in Water. *J. Chem. Phys.* **1972**, *57*, 495−504.
(53) Luukkonen, P.; Maloney, T.; Rantanen, J.; Paulapuro, H.; Yliruusi, J. Interaction — A Novel Approach Using Thermoporosimetry. *Pharm. Res.* **2001**, *18*, 1562−1569.
(54) Nakamura, K.; Hatakeyama, T.; Hatakeyama, H. Studies on Bound Water of Cellulose by Differential Scanning Calorimetry. *Text. Res. J.* **1981**, *51*, 607−613.

DOI: 10.1021/acs.biomac.7b01814
Biomacromolecules XXXX, XXX, XXX−XXX